ICES Journal of Marine Science Advance Access published April 14, 2015

ICES Journal of Marine Science

ICES International Council for the Exploration of the Sea
CIEM Conseil International pour l'Exploration de la Mer

ICES Journal of Marine Science; doi:10.1093/icesjms/fsv053

Onset, intensification, and decline of phytoplankton blooms in the Southern Ocean

Joan Llort[1]*, Marina Lévy[1], Jean-Baptiste Sallée[1,2], and Alessandro Tagliabue[3]

[1]*Sorbonne Universités (UPMC, Univ Paris 06)-CNRS-IRD-MNHN, LOCEAN Laboratory, 4 Place Jussieu, Paris F-75005, France*
[2]*British Antarctic Survey, Madingley Road, High Cross, Cambridge CB30ET, UK*
[3]*Department of Earth, Ocean and Ecological Sciences, School of Environmental Sciences, University of Liverpool, Liverpool L69 3GP, UK*

**Corresponding author: e-mail: joan.llort@locean-ipsl.upmc.fr*

Llort, J., Lévy, M., Sallée, J-B., and Tagliabue, A. Onset, intensification, and decline of phytoplankton blooms in the Southern Ocean. – ICES Journal of Marine Science, doi: 10.1093/icesjms/fsv053.

Received 17 September 2014; revised 4 March 2015; accepted 10 March 2015.

The seasonal cycle of phytoplankton biomass in the Southern Ocean (SO) is characterized by a period of rapid accumulation, known as bloom, that is typical of high-latitude regions. Recent studies have illustrated how spatial and temporal dynamics of blooms in the SO are more complex than in other oceans. This complexity is likely related to differences in vertical mixing and the iron availability. In this work, we examine the sensitivity of bloom dynamics to changes in vertical mixing and iron availability using a biogeochemical model. Under idealized physical forcing, we produce seasonal cycles of phytoplankton for an ensemble of SO scenarios and we describe the bloom dynamics in terms of the net biomass accumulation rate. Based on this metric, we define three crucial bloom phases: the onset, the climax, and the apex. For the ensemble of modelled blooms, onsets always occur in winter and can be either bottom-up (increase in productivity) or top-down (decrease in grazing) controlled. Climaxes are mostly found in spring and their magnitudes are bottom-up controlled. Apexes are always found in late spring and strongly top-down controlled. Our results show that while a "strict" onset definition is consistent with a winter onset, the surface spring bloom is associated with the climax of the integrated bloom. Furthermore, we demonstrate that onset phase can be distinguished from climax phase using appropriate bloom detection methods based on surface satellite-based products. The ensemble of these results suggests that Sverdrup's blooming conditions are not indicative of the bloom onset but of the climax. We conclude that the recent bloom onset debate may partly be due to a confusion between what is defined here as the bloom onset and the climax, and that the SO observed complexity is due to the factors that control the climax.

Keywords: bloom onset, iron, Sverdrup, Southern Ocean.

Introduction

The Southern Ocean (SO) is the largest high-nutrient low-chlorophyll region in the world's ocean. Its relatively low productivity has been attributed to a combination of iron scarcity (Martin *et al.*, 1990), elevated grazing, and light limitation (Boyd and Ellwood, 2010). Despite these unfavourable biological growth conditions, large accumulations of phytoplankton biomass, or blooms, are observed in surface waters each spring over wide areas of the SO (Thomalla *et al.*, 2011). The distribution of these blooms is very patchy in space and time. Hot-spots of phytoplankton accumulation are mainly seen where sources of iron are significant, i.e. in the lee of Islands (Moore and Abbott, 2000; Arrigo *et al.*, 2008). Additionally, the bloom onset dates are rather spread in time, from October to January (Thomalla *et al.*, 2011), and do not show a clear latitudinal pattern. This is unlike the pattern for North Atlantic spring bloom which is zonal and propagates from South to North (Siegel, 2002; Lévy *et al.*, 2005). The variability of bloom dynamics in the SO in terms of their amplitude, timing and location has been mainly documented from ocean-colour observations (Moore and Abbott, 2000; Arrigo *et al.*, 2008; Thomalla *et al.*, 2011). However, the drivers of the observed variability remains unclear. We hypothesize that patchy environmental conditions, involving zonally asymmetric mixed-layer distributions (Sallée *et al.*, 2010) combined with equally complex dissolved iron distributions (Tagliabue et al., 2011, 2014) are mostly responsible for the complex SO patterns.

Our current understanding of phytoplankton bloom dynamics mainly comes from works based on the North Atlantic. In this region, the mixed-layer, nutrient, and atmospheric environment are largely different from in the southern hemisphere. Historically, the emergence of blooms in the North Atlantic has been related to thinning of the ocean surface layer where turbulence is active (hereafter referred to as "turbulent or mixing-layer", or *XLD*, to be distinguished from the usual "mixed-layer depth", or *MLD*, which represents the upper-layer where hydrographical properties are well mixed; Franks, 2014). This thinning implied an increase of averaged exposure of phytoplankton cells to light (Gran and Braarud, 1935; Riley, 1942). Along with this bottom-up view, Sverdrup (1953) proposed that bloom would start when surface mixing-layer crosses a critical depth above which integrated phytoplankton growth would overcome phytoplankton losses (Siegel, 2002). It must be emphasized to note that Sverdrup (1953)'s hypothesis (also known as the Critical Depth hypothesis) is founded on the assumption that "within the top layer the turbulence is strong enough to distribute the plankton organisms evenly through the layer "(Sverdrup, 1953). This assumption is crucial to understand the Critical Depth hypothesis as points out that what matters for phytoplankton is the vertical profile of turbulent mixing, rather than the hydrographical properties of the water column. Indeed, the relevant parameter for the Sverdrup (1953)'s hypothesis is the *XLD* rather than the *MLD* (Franks, 2014).

As an alternative to the bottom-up understanding of ocean blooms, a top-down view has also appeared. This view proposes that, in essence, the causes of phytoplankton concentrations cannot be fully understood without considering the role of their main predator, zooplankton (Banse, 1994). The top-down hypothesis has gained interest recently via a series of papers that challenged the prevailing "bottom-up" paradigm (Behrenfeld and Boss, 2013). Using various tools (satellite data: Behrenfeld, 2010; float data: Boss and Behrenfeld, 2010; and model estimates: Behrenfeld *et al.*, 2013), it has been suggested that the North Atlantic spring bloom does not initiate in spring alongside thinning mixing-layers, but rather in winter when mixing-layer is deepening. This winter initiation is consistent with the hypothesis that dilution enables phytoplankton to better escape their predators and accumulate biomass (Evans and Parslow, 1985; Yoshie *et al.*, 2003; Marra and Barber, 2004).

In this context, our primary objective is to examine the drivers of phytoplankton blooms over the full range of SO environmental conditions. In particular, we examine how different environmental conditions (mixing-layer depth, ferricline, and solar radiation) result in bottom-up or top-down control. To that end, we extend a framework in which the rate of net biomass accumulation (r) results from a competition between growth (μ) and loss (l) of phytoplankton: $r = \mu - l = (1/P)(\mathrm{d}P/\mathrm{d}t)$, with P the total biomass of phytoplankton present in the water column (Riley, 1942; Sverdrup, 1953; Behrenfeld, 2010). At equilibrium, phytoplankton growth and loss are in balance and phytoplankton population remains stable. This balance can be disturbed by a sudden change in iron supply, light conditions, or stratification in isolation or in combination, which would then likely affect μ and l in different ways (Behrenfeld *et al.*, 2013). Our overarching question is how such perturbations modify μ and l at seasonal scale, and which term is the most sensitive to a given perturbation and the most effective at driving variations in r (i.e. phytoplankton population fluctuations). One of the key aspects of our approach is that we examine three important phases in the annual cycle of blooms: the bloom onset, climax, and apex. Using time evolution of r, we define these bloom phases as follows:

1. The bloom *onset* is when total biomass starts to accumulate.
2. The bloom *climax* occurs when the rate of biomass accumulation is maximal. After this instant, accumulation of phytoplankton continues but at a slower rate because ecosystem has yet started its way to readjustment (i.e. to recoupling).
3. Finally, the bloom *apex* marks the peak in total biomass, i.e. the time after which $l > \mu$ (recoupling is actually achieved) and accumulation starts decreasing.

Figure 1 illustrates these three phases associated with the time of minimum integrated biomass (onset), of maximum slope of integrated biomass (climax), and of maximum integrated biomass (apex). This distinction complements previous studies on bloom dynamics that focused either exclusively on onset (Sverdrup, 1953; Behrenfeld, 2010) or on climax (Lozier *et al.*, 2011; Ferrari *et al.*, 2014).

We address the question of bloom drivers in the SO in the framework of a numerical model. This model uses a state-of-the-art biogeochemical network (Aumont and Bopp, 2006) within a vertically discretized 1D water column configuration where vertical mixing is the main physical process. Aiming to examine the full range of SO conditions, we perform statistical analyses using an ensemble of 1200 model simulations with distinct seasonal cycles of mixing-layer depth, ferricline, and solar radiation. Bloom onset, climax, and apex dates are diagnosed for each run in the ensemble. Simultaneously, the distributions of variables such as iron supply, mixing-layer depth, light, phytoplankton growth, and loss rates for each of the three bloom phases are attributed to drivers. We investigate when bottom-up or top-down controls prevailed. This model allows us to test existing theories on bloom onset in an idealized and comprehensive framework, and to discuss them in the context of theSO. Furthermore, the completeness of the model data allows us to compare the onset and climax dates with the dates at which two different satellite-based bloom detection methods identify bloom initiation. These bloom detection methods are also compared with the date of the bloom onset predicted by Sverdrup (1953)'s hypothesis with the aim to evaluate at which point the validation (or refusal) of this hypothesis is influenced by the bloom detection method.

Methods

Biogeochemical model

The model was set up to represent the Permanent Open Ocean Zone (POOZ) of the SO, away from ice formation and melting, where nitrate and silica do not limit productivity. Our goal in this study is to untangle how the different phases of a bloom (onset, climax, and apex) are controlled by their physical and biogeochemical environment. As such, we deliberately chose to reduce the complexity of the problem by considering a 1D physical framework (e.g. lateral advection is neglected). Varying vertical diffusion reproduces seasonal cycle of the mixing-layer depth. Along with this idealized physical configuration, we model the associated biogeochemical activity with the model PISCES (Aumont and Bopp, 2006). PISCES contains 24 biogeochemical tracers with five nutrients able to limit phytoplankton growth: nitrate, phosphate, ammonium, iron, and silicate. The iron pool is explicitly modelled and controlled by a range of processes such as phytoplankton uptake, bacterial uptake, zooplankton, and bacterial recycling, remineralization and scavenging. In addition, four living pools are represented: two phytoplankton size classes (small and large) and two zooplankton size classes (microzooplankton and mesozooplankton). Large phytoplankton differs

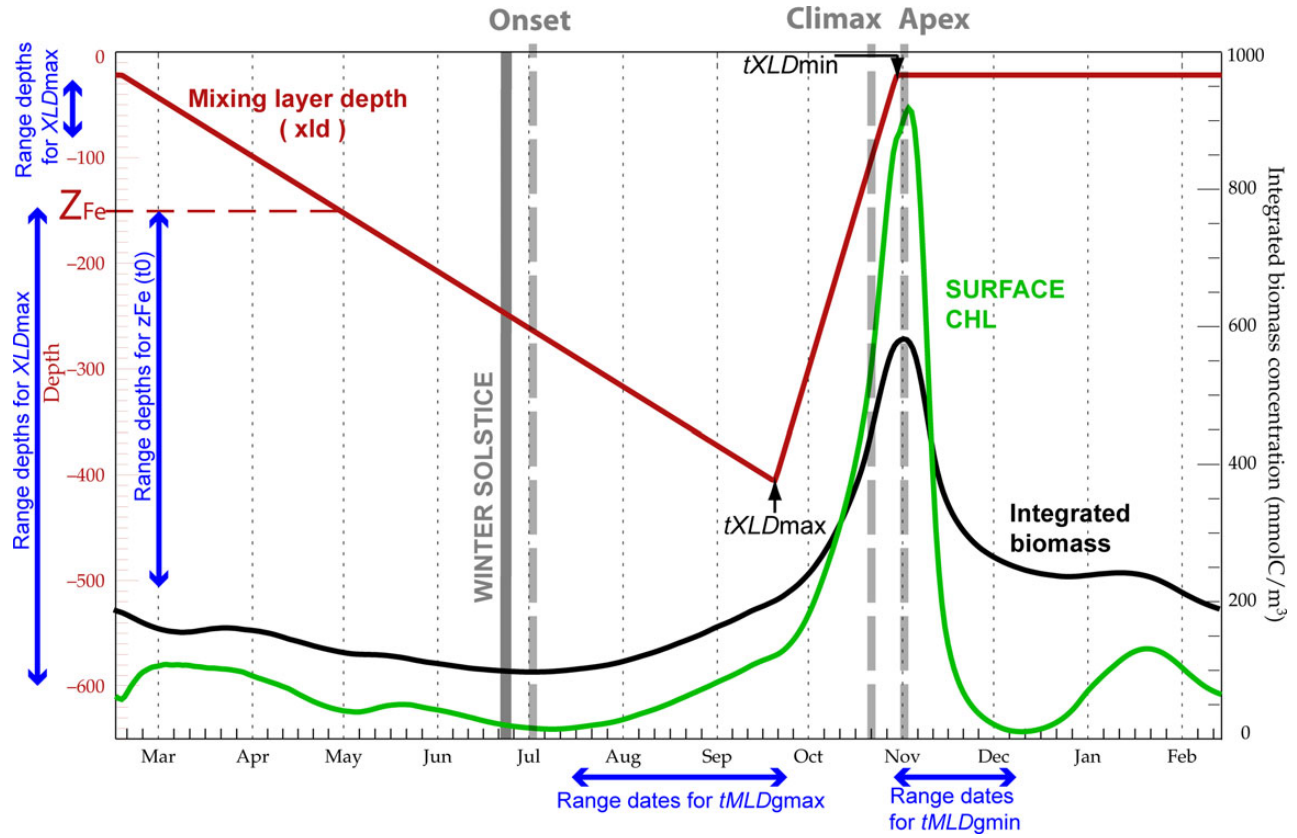

Figure 1. Seasonal cycle of the mixing depth (*XLD*; red line), integrated phytoplankton biomass (black line) and surface chlorophyll (green line) for one of the modelled blooms. The red horizontal dashed line marks the depth of summer ferricline (Z_{Fe}). The dates of the maximal and the minimal depth ($tXLD_{max}$ and $tXLD_{min}$, respectively) are indicated with a black arrow. The vertical grey solid line marks the date of the winter solstice (21 June) while vertical grey dashed lines mark the three bloom stages: onset, climax, and apex. Blue arrows show the range of values sampXLD_{min}led for each of the five physical parameters: maximal and minimal mixing dates (XLD_{max} and), its corresponding dates ($tXLD_{max}$ and $tXLD_{min}$) and the summer ferricline (Z_{Fe}).

from the small phytoplankton by higher requirements in iron and a greater iron half-saturation constant. Grazing pressure on each phytoplankton is also differentiated by size: microzooplankton (Z) preferentially grazes small phytoplankton while mesozooplankton (M) preferentially grazes the larger phytoplankton but also microzooplankton.

Prognostic equation for each phytoplankton group ($i = 1,2$) is:

$$\frac{\partial P_i}{\partial t} = \mu_i P_i - g^Z(P_i)Z - g^M(P_i)M - m_i P_i + \frac{\partial}{\partial z}\left[\kappa_z \frac{\partial P_i}{\partial z}\right], \quad i = 1, 2, \tag{1}$$

where P_i is the phytoplankton biomass, μ_i is the growth rate, g_i represents the grazing rate, and m_i is the mortality rate. The last right hand side term is the effect of vertical diffusion over biomass due to vertical mixing of intensity κ_z. The growth rate (μ_i) is computed as follows:

$$\mu_i = \mu_{\max} f_i(T) h(z)\left(1 - \exp\frac{-\alpha_i Q_i^{\mathrm{Chl}} \mathrm{PAR}_i}{\mu_{\max} f_i(T) L_i}\right) L_i, \quad i = 1, 2 \tag{2}$$

where $f_i(T)$ is the dependence of the growth rate with temperature (Eppley, 1972), $h(z)$ is a penalization term for deep mixing, PAR_i is function of the shortwave radiation at the surface, α_i is the initial slope of the photosynthesis-irradiance curve, Q_i^{Chl} the Chl:C quota for each phytoplankton, and L_i is the nutrient limitation. Nutrients limitation in our set-up can only be due to Fe, so $L_i \equiv L_i^{\mathrm{Fe}}$, where

$$L_i^{\mathrm{Fe}} = \min\left(1, \max\left(0, \frac{Q_i^{\mathrm{Fe}} - Q_{i,\min}^{\mathrm{Fe}}}{Q_{i,\mathrm{opt}}^{\mathrm{Fe}}}\right)\right). \tag{3}$$

Iron limitation is formulated following a *Quota* approach (McCarthy, 1980; Droop, 1983) with the term $Q_{i,\mathrm{opt}}^{\mathrm{Fe}}$ allowing luxury uptake (as in Buitenhuis, 2010). Grazing rate by zooplankton is computed as a Michaelis–Menton parametrization with a phytoplankon feeding threshold (Aumont and Bopp, 2006). It can be formulated as follows:

$$g^Z(P_i) = g_m^{0,Z} f_Z(T) \frac{\gamma_{P_i}^Z}{K_{\mathrm{graz}}^Z + \sum_{P_i} \gamma_{P_i}^Z P_i} F_{\mathrm{thresh}}^{Z,P_i}, \tag{4}$$

where Z stands for both micro- and mesozooplankton, $g_m^{0,Z}$ is the maximum grazing rate at 0°C, $f_Z(T)$ is a temperature-dependent function, K_{graz}^Z is the corresponding half-saturation constant, $\gamma_{P_i}^Z$ is the preference of each zooplankton for each phytoplankton, and $F_{\mathrm{thresh}}^{Z,P_i}$ is a function computing the corresponding feeding thresholds

for each couple phyto/zoo. Encounter probability between grazers and phytoplankton is not explicitly computed but results from the volumetric concentration of the four biological compartments.

The model equations were computed on a regular vertical grid of 74 + 1 vertical levels (constant spacing of 7 m for the first 74 levels and a last one of 500 m depth) and a time step of 20 min. The vertical mixing coefficient (κ_z), temperature and surface photosynthetic available radiation (PAR) were analytically prescribed every 6 h. Vertical mixing coefficient were assumed to be constant and equal to 1 $m^2\ s^{-1}$ within a surface mixing layer of depth *XLD*, and equal to $10^{-5}\ m^2\ s^{-1}$ below. Hence, in this study, *XLD* was not calculated but imposed through the κ_z vertical profile. The extremely large value of κ_z within the *XLD* guaranteed that turbulence was strong enough to homogeneously distribute phytoplankton (i.e. Sverdrup, 1953s assumption). Following Lévy (2015), who highlighted the need to represent the full seasonal cycle of the *XLD* to study the bloom, we imposed an idealized seasonal cycle of the *XLD* divided into three phases (red curve in Figure 1):

- A fall/winter phase of convection and progressive *XLD* deepening.
- A spring phase where cessation of convection led to the thinning of the *XLD*.
- A summer phase with a relatively shallow and constant *XLD*.

To ensure that the timing of these phases and the magnitude of the *XLD* were relatively realistic, we used data estimates derived from Argo data (Sallée *et al.*, 2010). These data provided us with an estimate of the depth of the seasonal thermocline in the SO, which we assumed to reflect the mixing depth. Sub-seasonal variability in the *XLD* was not accounted for. For temperature and surface PAR, we used a smoothed climatological seasonal cycle constructed from observations (DFS3-ERA40; Broderau *et al.*, 2008) averaged over the 40–60°S latitudinal band.

The summer initial condition for dissolved Fe profile was constructed by assuming low concentrations (0.03 nMolFe/l) above a prescribed ferricline depth (Z_{Fe}), and larger concentrations (0.5 nMolFe/l) below. The depth of the ferricline for the initial condition iron profile is one of the parameters we varied in our set of simulations. It is generally understood that the summer Fe profile is set by a combination of remineralization, scavenging and physical supplies by lateral sources. While remineralization and scavenging are parametrized in PISCES, there remains a large degree of uncertainty in the parameterization. In addition, lateral supplies were not explicitly accounted for. To overcome these issues and to allow the model to reach a repeating and stationary seasonal cycle, the dissolved iron profile was restored towards its initial value at the end of each summer.

Initial vertical profiles for macronutrient (i.e. nitrates, phosphates, and silicates) were constructed based on the winter mean profiles collected during the KERFIX project (Jeandel *et al.*, 1998). This project aimed to monitor ocean-atmosphere CO_2 and O_2 exchanges and related processes with a time-series station (called KERFIX station) located at 50°40′S–68°25′E, 60 miles southwest of the Kerguelen Islands (SO). From January 1990 to March 1995, regular monthly measurements of physical and biogeochemical water properties were carried out at KERFIX station. As for iron, macronutrients were restored to the initial profiles at the end of each summer. Initial conditions for the four living compartments were set to low values for the first year. The simulations were integrated for 3 years, starting in austral summer (15 February), with outputs saved at daily frequency. A repeating seasonal cycle was reached after 2 years and results are based on the third year of simulation. As an example, Figure 1 shows a complete seasonal cycle of integrated biomass (black curve), surface Chl (green), *XLD* (red), and summer Z_{Fe}, for one of these runs.

Ensemble runs

An ensemble of runs was performed by varying the *XLD* and summer Z_{Fe} in the range of values found in the POOZ. Specifically, these *XLD* and Z_{Fe} were modified based on the following variables:

(i) The winter maximal mixing depth (XLD_{max})
(ii) The summer minimal mixing depth (XLD_{min})
(iii) The date at which XLD_{max} was reached ($tXLD_{max}$)
(iv) The date at which XLD_{min} was reached ($tXLD_{min}$)
(v) The summer ferricline depth, Z_{Fe}

The variables i–v were set based on a discrete set of observed values, with equal weight given to each discrete value (see ranges in Figure 1, blue arrows). The ranges for Z_{Fe} were established based on a recent compilation of dissolved iron measurements (Tagliabue *et al.*, 2011), the ranges of values used to set *XLD* were based on >500 000 density profiles sampled in the SO by Argo floats data (Sallée *et al.*, 2010). Our choice of variables led to an ensemble of almost 1200 different scenarios that combine different values of the above parameters i–v covering a wide range of *XLD* and Z_{Fe} observed in the SO.

In our model, the amount of Fe injected at the surface each year was not prescribed: Fe was entrained in the mixing layer during the deepening phase. Thus, the Fe supply depended on the relative depths of the ferricline and XLD_{max} (Figure 2). The relationship between both variables was however non-linear, due to the effects of consumption/remineralization by the biological community and the rate of stratification/destratification. A peculiarity of the SO is that the ferricline depth is often found below the maximum

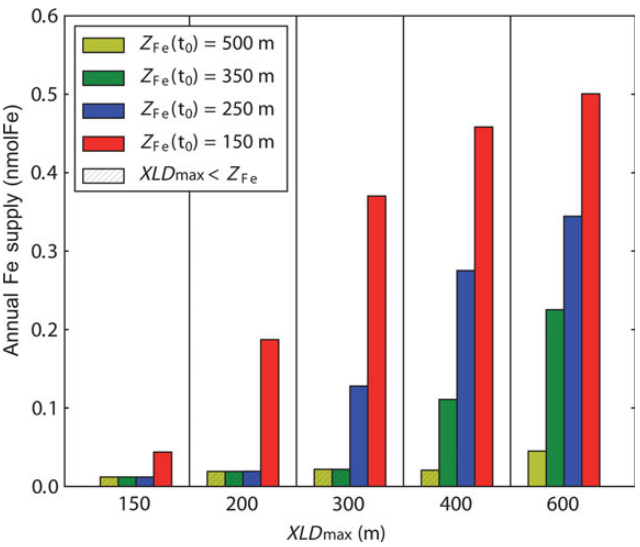

Figure 2. Histogram of the total amount of Fe supplied to the 0–50 m surface layer as a function of the XLD_{max} and the summer ferricline (colours).

winter mixed-layer depth (Tagliabue *et al.*, 2014), implying some regions permanently Fe-limited despite strong and deep winter mixing. In our scenarios, this situation occurred when Z_{Fe} was greater than XLD_{max} (Figure 2). Note that this is different from other high-latitude productive regions such as the North Atlantic, where nitrate is the main limiting nutrient. In the North Atlantic, the depth of winter mixing and the convective nitrate supplies are more tightly correlated than its SO counterpart (depth of winter mixing and convective Fe supplies).

Bloom onset, climax, and apex

The bloom phenology was decomposed into three main events defined by the rate of net biomass accumulation (r), which writes as:

$$r = \frac{1}{P^{int}}\frac{dP^{int}}{dt}, \quad \text{with} \quad P^{int} = \int_0^H P dz \tag{5}$$

where H is the depth of the water column. For simplicity, hereinafter we will refer to P^{int} as P. From the seasonal evolution of r, we defined the bloom onset (total biomass starts to increase: P_{min}, $r = 0$, and $r' > 0$; hereafter all temporal derivatives are marked by a prime, i.e. $r' = \partial r/\partial t$); the bloom climax (the rate of accumulation is maximum: $r = r_{max}$ and $r' = 0$) and the bloom apex (bloom peaks in total biomass: $P = P_{max}$, $r = 0$ and $r' < 0$). See Figure 1 where the three steps are reported. We note here that r was computed in our study from a total water column integral, which slightly differs from what is done in Sverdrup (1953) or Behrenfeld (2010) where P was integrated down to the base of the mixing layer. As Chiswell (2013) pointed out, mixing layer integration of P might be misleading when the mixing layer restratifies as plankton is not conserved in the *XLD*. Integrating over the whole water column overcomes the discontinuity issue pointed out by Chiswell (2013).

Integrating Equation (1) and dividing all terms by P, r can be written as the integrated balance between phytoplankton source (i.e. growth rate, μ) and sinks (i.e. grazing and mortality rates, g and m, respectively):

$$r = \mu - g - m. \tag{6}$$

Hence, the evolution of modelled ecosystem in the water column can be synthesized as:

$$r = \mu - l, \tag{7}$$

where μ is the mean growth rate of the total depth integrated phytoplankton community, and l is the sum of grazing and mortality.

Bloom timing

In our set of experiments, the time of the deepest convection ($tXLD_{max}$) can vary by up to 2 months between experiments, and the time at which summer stratification is reached ($tXLD_{min}$) by 1 month (Figure 1). To account for this variability, the timing of the different bloom phases was not only measured relatively to the day of the year but also relatively to the phase of the physical forcing (i.e. relative to the time of $tXLD_{min}$ and $tXLD_{max}$). In this sense, bloom phases before $tXLD_{max}$ occurred in "winter", when the mixing layer is still deepening. Similarly, bloom phases occurring between $tXLD_{max}$ and $tXLD_{min}$ are occurred during the spring thinning of the mixing layer.

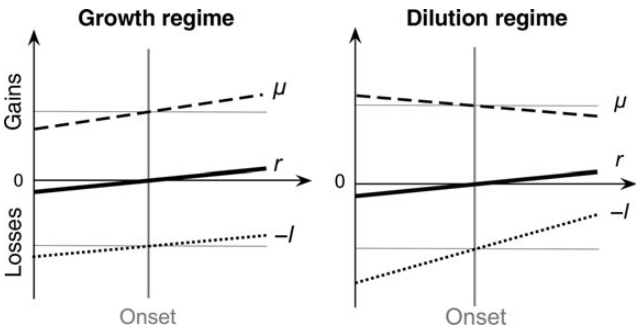

Figure 3. Diagram of the two mechanisms able to trigger the bloom in winter. In growth (dashed), net accumulation (solid) and losses (dotted) rates are represented for the (a) Growth Regime and (b) the Dilution Regime. Losses rate is represented as negative ($-l$) to illustrate the balance $r = \mu - l$. The vertical grey line marks the date of onset at which r becomes greater than zero.

Bottom-up vs. top-down control

In this paper, we aim at investigating whether the bloom seasonal cycle is controlled by bottom-up or top-down processes. Here, we detail how the relative intensity of μ' and l' can be used to link onset, climax, and apex to their bottom-up or top-down controls.

Onset ($r = 0$, $r' > 0$) occurs when gains first overcome losses. At onset integrated phytoplankton biomass is minimal and losses are always decreasing. Under these circumstances, two possible mechanisms can cause the bloom onset (Figure 3):

1. *Growth regime*: The growth rate has already started to increase while the loss rate is still decreasing or stable. The growth will then become larger than loss at some point leading to the initiation of net biomass accumulation in the water column (i.e. $r > 0$). The onset is controlled by the growth (i.e. light and nutrients) and therefore is bottom-up driven. Analytically, this regime can be expressed as:

$$\mu' > 0, l' \leq 0 \Rightarrow r' > 0. \tag{8}$$

2. *Dilution regime*: Growth and loss rate are decreasing due to nutrients depletion, low light conditions, and *XLD* deepening. The latter causes the dilution of plankton (both, phyto- and grazers) when increasing the volume of water in the mixing layer. This process strongly decreases the prey–predator encounter probability causing a faster decrease on loss rate than on growth rate. The grazing pressure relaxation allows phytoplankton ecosystem to start increasing. This regime is top-down controlled and it corresponds to bloom onset scenario described in Marra and Barber (2004), Behrenfeld (2010), and Boss and Behrenfeld (2010). It can be analytically expressed by

$$l' < \mu' < 0 \Rightarrow r' > 0. \tag{9}$$

Climax ($r = r_{max}, r' = 0$) marks the instant of the fastest population increase. Consequently, climax is the inflection point in the seasonal evolution of biomass:

$$r = r_{max} \Rightarrow r' = 0 \quad \text{where } P'' \propto r'. \tag{10}$$

From an ecosystem point of view, this means that the trend in loss rate overcomes the trend in growth rate ($l' \geq \mu'$). Therefore, the

bloom climax marks the beginning of the recoupling process that leads to the re-equilibrium of the system. Climax can be achieved in two different ways: either μ' becoming negative due to nutrient limitation (bottom-up control) or l' becoming greater than μ' (top-down control).

Finally, *apex* ($r = 0, r' < 0$) marks the actual time of recoupling, when losses first equals gains. At apex, losses are always increasing $l' > 0$. Apex can be reached when growth is still increasing, and biomass accumulation is stopped by grazers (i.e. $l' > \mu'$ with $\mu' > 0$); we refer to this case as the top-down controlled. In the bottom-up case, the apex is mainly due to change on the growth rate trend (i.e. $\mu' < 0$). This situation is often caused by the nutrients depletion in the mixing layer. We note that both top-down and bottom-up controls can mutually act together. Our analysis only points out the dominant process at play.

Bloom onset detection and Sverdrup's hypothesis

With the aim to evaluate how onset and climax phases can be detected using ocean-colour data, we applied two different bloom detection methods to model outputs. Several bloom detection methods exist in the literature and it has been shown that bloom detection dates can strongly differ depending on which method is applied (Ji *et al.*, 2010; Brody *et al.*, 2013). Here we use two methods, a surface biomass- (sP) and a surface chlorophyll- (sChl) based methods, that have already been implemented in literature with ocean-colour data (Behrenfeld, 2010; Brody *et al.*, 2013). Despite these methods are designed to be applied with ocean-colour data, in our case bloom detection dates are obtained from modelled sP and sChl and compared to the actual onset and climax computed from the full vertical profile. The two bloom detection methods are defined as follows:

1. P^*-method: date at which $P^{*\prime} > 0$ Behrenfeld (2010), where:

$$P \approx P^* = sP \times XLD \text{ while } t < tXLD_{\max}. \tag{11}$$

2. sChl-method: Date of maximal sChl" (Sallée *et al.*, 2015, in this issue)

The P^*-method is based on a depth integrated view of the bloom: it estimates the amount of biomass within the water column assuming that phytoplankton is homogeneously mixed in the ocean upper layer and that the amount of biomass below is negligible. Onset is then detected when integrated biomass starts to increase. On the other hand, the sChl-method is only based on the surface imprint of the bloom and onset detection is based on the rate of change of sChl. Interestingly, when used in the literature, the P^*-method resulted on bloom onset detected in winter (Behrenfeld, 2010) while sChl-method detects bloom onsets mostly in spring (White *et al.*, 2009; Sallée *et al.*, 2015).

A number of studies have addressed high-latitude blooms using ocean-colour data with the aim to validate (or to reject) Sverdrup (1953)'s hypothesis (Siegel, 2002; Behrenfeld, 2010; Chiswell, 2011). Here, we aim to quantify at which point the validation (or refusal) of the Sverdrup (1953)'s hypothesis depends on the bloom detection method implemented. We took advantage of the model data completeness to compute the critical depth (Z_c) based on the two main Sverdrup (1953)'s assumptions: strongly turbulent surface layer and constant mortality (assumed to be the main loss term in winter–early spring). The formal expression of Sverdrup (1953) critical depth (as presented in Lévy, 2015, in this issue)

$$\frac{\alpha I_0}{kZ_c}(1 - e^{-kZ_c}) = m \tag{12}$$

can be approximated to

$$Z_c \approx \left(\frac{1}{k}\right)\frac{\mu_0}{m}, \tag{13}$$

where μ_0 is the phytoplankton growth rate at surface (i.e. $\mu_0 = \alpha I_0$), k is the light attenuation coefficient (in m^{-1}), and m is the mortality rate. The variable Z_c is computed at each time step using the model outputs for μ_0, m averaged from August to October and a light attenuation coefficient of $k = 0.05\ m^{-1}$, constant throughout the year (i.e. no phytoplankton shelf-shading; Lévy, 2015). Determining the date at which $XLD = Z_c$ for each modelled bloom, we are able to investigate whether Sverdrup's bloom conditions are satisfied or not for the two surface bloom detection methods presented above (P^*-method and sChl-method).

Results

Abrupt and smooth blooms

Two types of bloom phenology emerge from our 1200 runs ensemble: abrupt blooms, characterized by a sudden and very strong intensification of biomass accumulation, and smooth blooms, which display a smoother biomass accumulation. In fact, there is a continuous range of possible phenologies between these two bloom types and, hence, no objective method that distinguishes them. Nevertheless, as abrupt blooms reach, by definition, a higher value of r at climax, the 20% of blooms with the largest $r_{\max}$ were identified as abrupt, and the remaining 80% as smooth in the following analysis. Importantly, these two types of SO bloom phenologies are also identifiable from ocean-colour observations (Sallée *et al.*, 2015).

For illustrative purpose, we will describe an example of an abrupt and smooth bloom taken from our results (Figure 4). In the abrupt case example (Figure 4a, c, and e), the *XLD* reaches 400 m in winter and the summer ferricline is located at 150 m. This deep winter mixing causes strong light limitation over 6 months of the year (from May to October; yellow surface in Figure 4e). Simultaneously, Fe limitation (red surface in Figure 4e) declines as *XLD* becomes deeper than Z_{Fe} and entrains Fe to the surface. The bloom onset occurs around 1 July and is followed by 2.5 months of a low and stable positive r during which the *XLD* continues to progressively deepen. We will refer to this period as the *plateau*. Then, when $tXLD_{\max}$ is reached and the *XLD* starts shallowing, r rapidly increases until climax ($r_{\max}$) is reached on 20 October. In this scenario, the climax is an abrupt and strong peak that occurs during the period of *XLD* restratification. This date also marks the start of a large and rapid increase in both integrated biomass (P) and surface chlorophyll (sChl) (black and green lines in Figure 4a). Apex is reached 10 days after the climax (1 November) associated to a rapid decline in r, which is driven by decreasing μ as Fe-limitation becomes important, as well as increasing losses ($l' \gg 0$). Following apex, growth/loss equilibrium ($r \approx 0$) is re-established over the summer (i.e. grazers-prey recoupling). This type of bloom is characteristic of high-latitude regions like the North Atlantic and iron rich waters of the SO (Waniek, 2003).

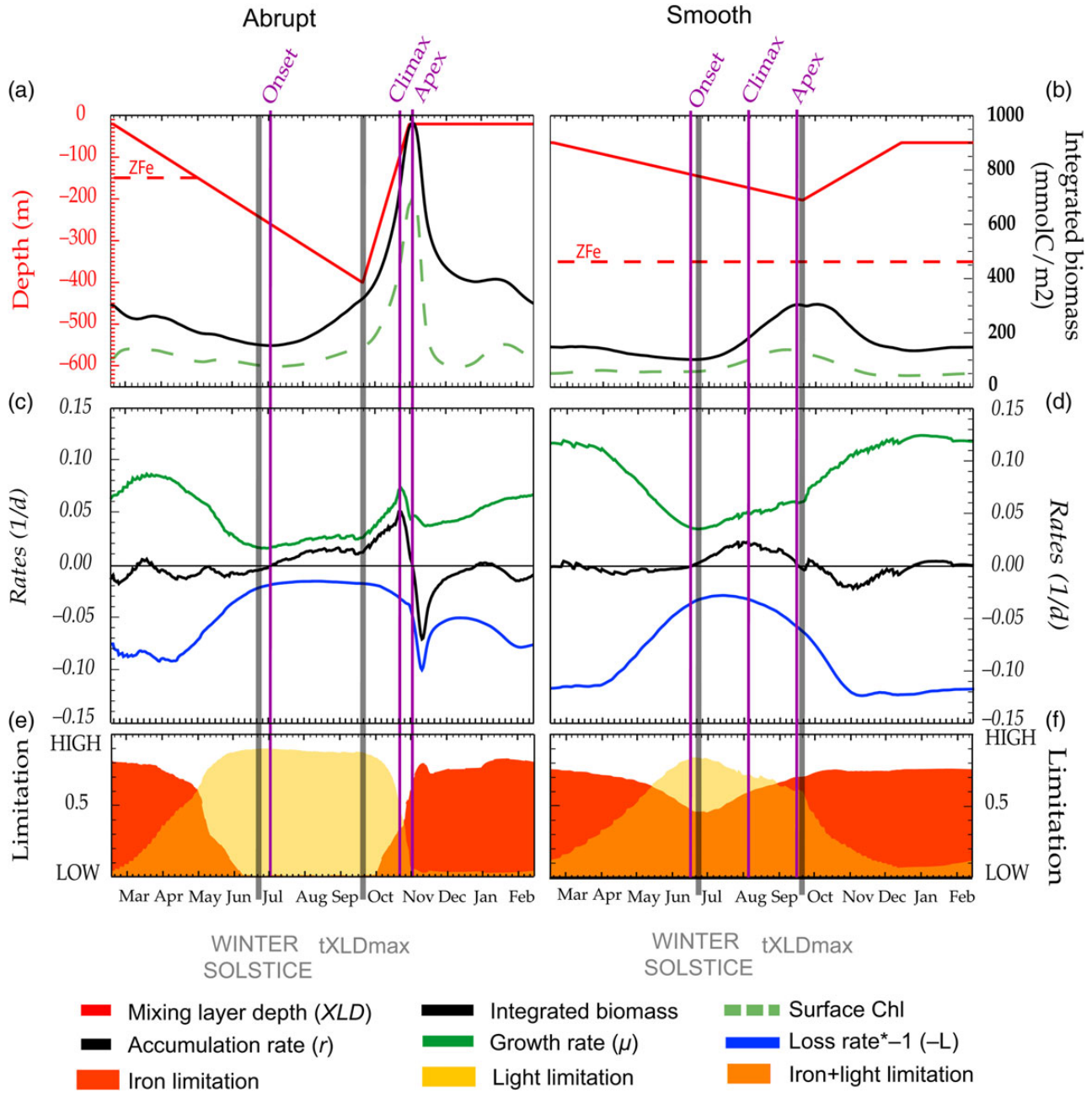

Figure 4. Seasonal cycle of the forcing *XLD* (red line) and model outputs of integrated biomass (black line) and surface chlorophyll (green line) for (a) an abrupt bloom and (b) a smooth bloom. Summer Z_{Fe} is indicated by a horizontal red dashed line. The seasonal cycle of the accumulation rate (r, black line), the growth rate (μ, green line), and losses rate (l, blue line) for both runs are represented in panels (c) and (d). Losses rate is represented as negative ($-l$) to illustrate the balance $r = \mu - l$. Limitation due to Fe and light are shaded in red and yellow areas; orange areas stands for the time at which both factors are limiting. Winter solstice date and XLD_{max} date are indicated by a vertical grey line. Onset, climax, and apex dates for each run are marked by a light blue dashed line.

In the smooth bloom case example (Figure 4b, d, and f), *XLD* reaches 200 m in winter, with a long period of restratification (>2 months) and a relatively deep mixing during summer (65 m). The variable Z_{Fe} is deeper than XLD_{max}, so mixing does not reach the largest Fe stocks, which maintains a significant Fe limitation all year-round. As for abrupt bloom case, onset occurs in mid-June and is followed by a *plateau* phase which lasts during *XLD* deepening. In contrast to the abrupt bloom (Figure 4a, c, and e), the *plateau* has a much smoother shape and, instead of switching to a high r phase, is followed by a phase where r declines slowly. Climax is in late-July, in the midst of the *plateau* and just before $tXLD_{max}$; the accumulation intensity at climax is almost four times lower than for the abrupt bloom case ($r_{max}^{smooth} = 0.02\,d^{-1}$ compared with $r_{max}^{abrupt} = 0.075\,d^{-1}$). Restratification is not associated with an increase in accumulation, which is likely due to prevailing Fe limitation. The climax lead to the beginning of recoupling and apex is

reached after 2 months (around mid-September), associated to a strong grazing pressure that overcomes the steady increase in growth rate (at $r = 0 : l' > \mu' > 0$, Figure 4b–d). Overall, the temporal changes in r are much less pronounced than for the abrupt case (Figure 4a–c) and the apex seems to arise from the long process of re-equilibrium that begins just after the onset, due to maintained top-down control. The variables P and sChl display a weak seasonal cycle with maximal values between September and October. The maximal value of sChl is reached just before P_{max}, which in contrast to the abrupt bloom case, has a broader and lower peak. This second type of bloom are often observed in subtropical regions and low iron concentration areas of the SO.

Bloom seasonal cycle: onset, climax, and apex

Onset

A remarkably consistent result over our 1200 simulations is that in 100% of the situations that we have explored, the bloom onset always occurs in winter, when the mixing layer is deepening (Figure 5a). The median value of the onset date is ∼2 months before $tXLD_{max}$ and 4 months before $tXLD_{min}$. Abrupt blooms tend to initiate earlier than smooth blooms, and the spread of the time of initiation is wider for smooth blooms than for abrupt blooms.

As introduced above, these winter onsets can either be growth or dilution driven. Here we assess each of the blooms in terms of the rate of change in losses and growth (l' and μ', respectively) at the time of onset (Figure 6). In this way, we can discriminate between the bottom-up (increase in growth rate or Growth regime) and top-down (decrease in grazing or Dilution regime) control. Overall, across the 1200 scenarios of our study we find an equal distribution between Growth regimes ($\mu' > 0$, red quadrant in Figure 6) and Dilution regimes ($\mu' < 0$, blue semi-quadrant in Figure 6). No significant differences in the onset regime are found for abrupt blooms (represented by triangles in Figure 6).

In terms of absolute timing, all onsets occurring after the winter solstice are associated to Growth regimes and those occurring before the winter solstice, to the Dilution regime (see colour bar in Figure 6). Thus, in our simulations (and unlike the results of Behrenfeld *et al.*, 2013 in a model of the North Atlantic) dilution is not always efficient enough to initiate the bloom. We found that the efficiency of dilution at initiating the bloom is related to the speed of destratification of the mixing layer. Dilution is efficient

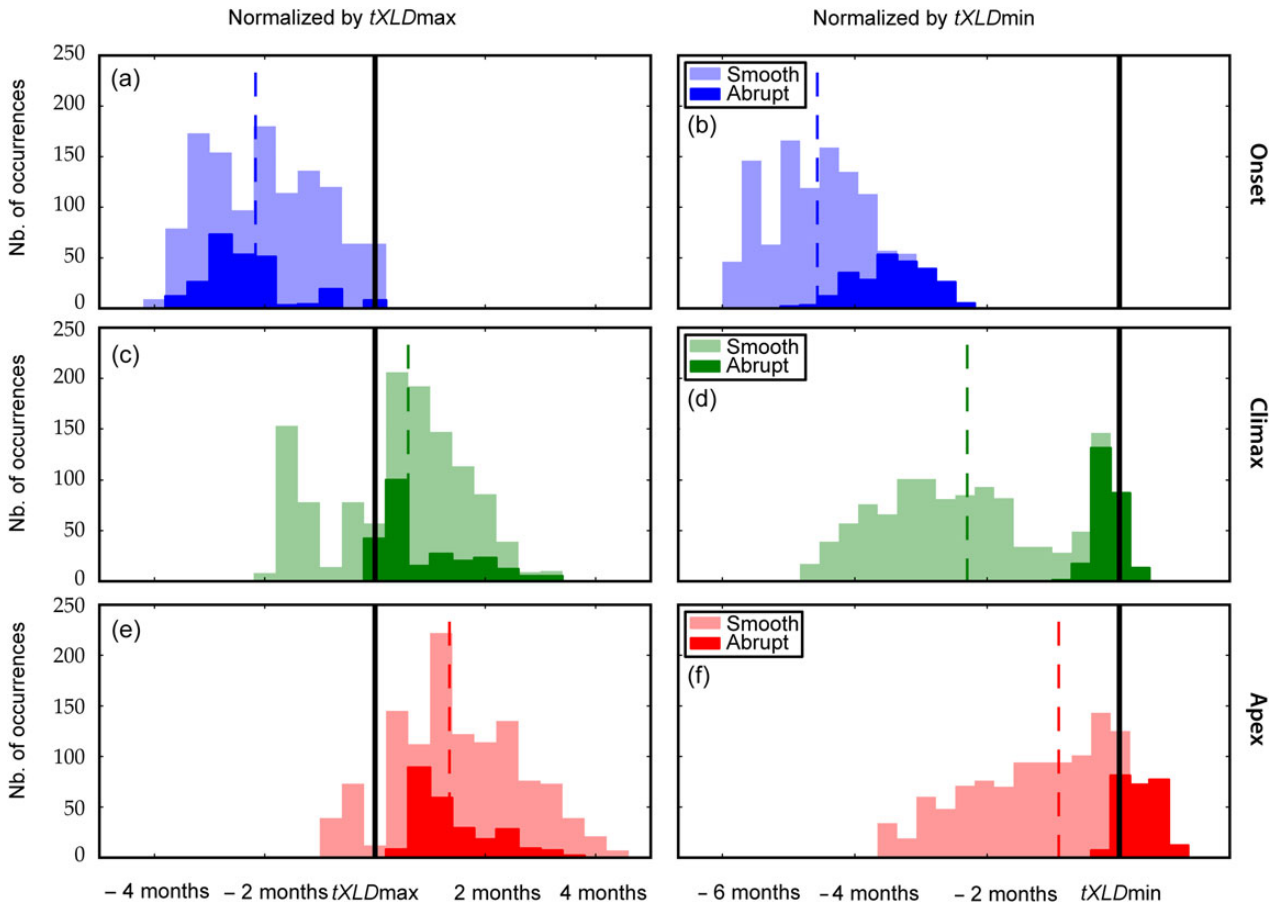

Figure 5. Bloom onset, climax, and apex dates for each modelled bloom have been normalized by the corresponding $tXLD_{max}$ (left column) and $tXLD_{min}$ (right column). In the figure, the histogram of the ensemble of modelled blooms representing: (a) the onset date normalized to the $tXLD_{max}$ date, (b) the onset date normalized to the $tXLD_{min}$ date, (c) the climax date normalized to the $tXLD_{max}$ date, (d) the climax date normalized to the $tXLD_{min}$ date, (e) the apex date normalized to the $tXLD_{max}$ date and (f) the apex date normalized to the $tXLD_{min}$ date. Median value is represented by a vertical dashed line. Abrupt blooms distribution are in dark colour and smooth blooms distribution in light colour. Normalization allows to identify the link the bloom phase with the dynamics of the *XLD*. For instance, independently of the absolute onset date, negative values represent onsets occurring before $tXLD_{max}$ (i.e. before the start of stratification) while positive values indicate that bloom starts after $tXLD_{min}$ (i.e. during stratification).

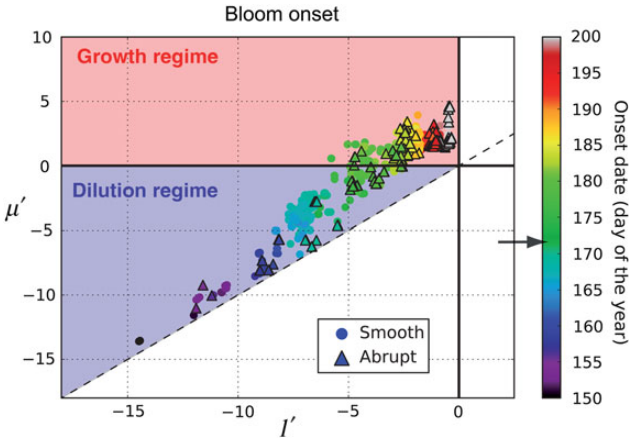

Figure 6. Growth and losses rate trends at the date of onset for the ensemble of modelled blooms. Circles stand for smooth blooms and triangles for abrupt blooms. Growth Regime quadrant (background red shade) and Dilution regime semi-quadrant (background blue shade). The absolute onset date (day of the year) is represented by coloured symbols. Austral winter solstice date (21 of June, day of the year 172) is marked with an arrow on the colour bar.

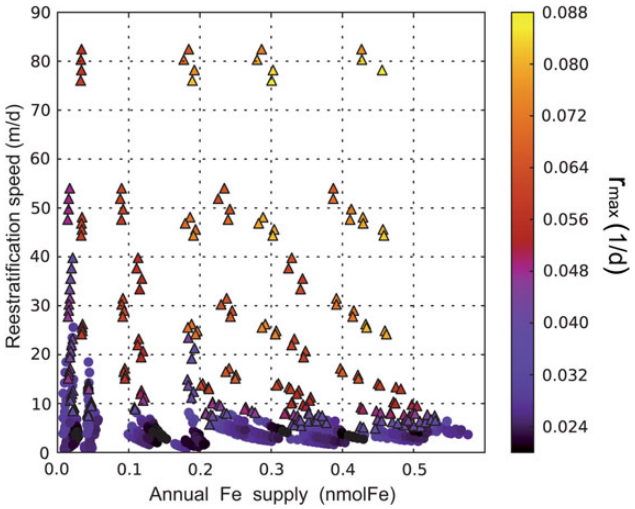

Figure 7. The climax intensity (or r_{max}; in d^{-1}) is represented in colour as a function of the vertical iron supply and the reestratification speed. Circles stand for smooth blooms and triangles for abrupt blooms.

when the destratification is strong enough to dilute predators, but weak enough to retain favourable light conditions for phytoplankton. In our simulations, we find a threshold between dilution and Growth regimes of at $\approx$2 m d^{-1} (not shown). When the destratification rate is greater than $\approx$2 m d^{-1}, the decrease in losses due to dilution is not strong enough to overcome the decrease in growth and to cause the bloom to onset. In this case, the onset is delayed until light conditions become more favourable (i.e. after winter solstice), switching to a Growth regime. Alternatively, when the destratification rate is less than $\approx$2 m d^{-1} the opposite occurs, favouring Dilution regime.

Climax

After the bloom onset, biomass accumulation increases until it reaches a maximum rate that we define as the climax (time of $r = r_{max}$). We note here that this date is different from the date of maximal biomass stock: accumulation continues until r switches back to a negative value. Instead, climax refers to the maximum increase rate of integrated biomass. In contrast to the bloom onset, for the large majority of blooms ($\approx$80%), climax is reached during the phase of *XLD* retreat, i.e. after XLD_{max} (Figure 5c). The remaining 20% of blooms are characterized by a climax before or when the mixing-layer reaches its maximum depth. However, all these blooms with a climax before XLD_{max} are smooth blooms. Abrupt blooms, associated with, by definition, a large (i.e. an "intense" climax) have their climax occurring after XLD_{max}.

Interestingly, for all seasonal cycles analysed, we found the accumulation reaches its maximum before the surface layer re-stratifies to its minimal value (Figure 5d). In summary, we find that in 80% of our simulation climax occurs during the spring stratification (i.e. before $tXLD_{min}$ and after $tXLD_{max}$). In addition, climax associated with all the abrupt blooms occurs at the time where the mixing layer reaches its minimal value (i.e. at $tXLD_{min}$ and after $tXLD_{max}$; dark green in Figure 6c and d). These results suggest a relationship between climax date and intensity, and the surface layer re-stratification period, which in turns points out the possible importance of light on biomass accumulation rate. Therefore, we find that the faster is the restratification of the surface layer, the larger is the maximum accumulation rate (Figure 7), with the total Fe input playing a secondary role. We note that for a given restratification speed (except for the very low restratification, slower than 5 m d^{-1}), r_{max} is tightly linked to the total Fe input in the surface layer. We interpret the tight relationship between r_{max} and the restratification as an indication of bottom-up control: a rapid improvement in light conditions leads to a parallel increase in growth rate (μ), which quickly translates into a rapid elevation of r, as grazers are not able to respond at the same rate. The amount of Fe available in winter thus works as a catalyst, allowing phytoplankton to take an optimal benefit of the increase in light conditions.

Apex

The apex date is reached when loss rate first overcomes growth rate ($l = \mu$) causing biomass accumulation to arrest ($r = 0$). For 90% of the scenarios we analysed, apex occurs after the mixing layer reaches its maximum (median value $\sim$1.5 months later; Figure 5e). In addition, apex is reached, in >75% of bloom scenarios, before the date of minimum mixing depth (median value $\sim$1 month before; Figure 5f). However, apex for abrupt blooms occurs after $tXLD_{min}$ (hence also after $tXLD_{max}$; Figure 5e and f). Such blooms can be viewed as examples of "bloom and bust" dynamics occurring during a rapid restratification that causes a sudden drop in r following the climax (compare Figure 5d and f; dark colours, or example of Figure 4b).

By assessing the state of the ecosystem at the apex date, we can better understand the processes leading to this stage. At apex, l' is always positive (Figure 8), which means grazing pressure is increasing. In contrast, μ' can be either positive (but necessarily lower than l') or negative (Figure 8). Over the ensemble of scenarios, 68% have an increase in growth ($\mu' > 0$) at the time of apex, and 32% have a decrease in growth ($\mu' < 0$) at the time of apex. However, l' is always greater than μ' (up to a factor 10 in some cases) indicating strong top-down control for our entire suite of scenarios. The earliest apex dates are always associated with $\mu' > 0$ (Figure 8), while after around day 260 ($\sim$mid-September), μ' can either be positive or negative at recoupling. The highest loss rates ($l' > 100$ d^{-1}) are always associated to abrupt blooms (see triangles in Figure 8).

Relating bloom phases and bloom detection methods based on surface Chl

Many of the seasonal cycles generated by our model are characterized by a *plateau* phase, with positive, but weak and relatively constant accumulation between onset and climax (see Section Abrupt and smooth blooms and Figure 4). While in terms of biomass accumulation, the bloom has definitely started (i.e. r), there is little accumulation of chlorophyll at the ocean surface (sChl; see examples in Figure 4, green dashed curve). Clearly, detecting bloom onset from surface chlorophyll observations would be challenging in such cases. In this section, we aim to evaluate two bloom detection methods that have been previously applied to surface observations of Chl accumulation (e.g. Behrenfeld, 2010; Brody *et al.*, 2013), see what phase of the bloom they detect (onset or climax) and if they comply to the critical depth hypothesis or to the dilution/recoupling hypothesis.

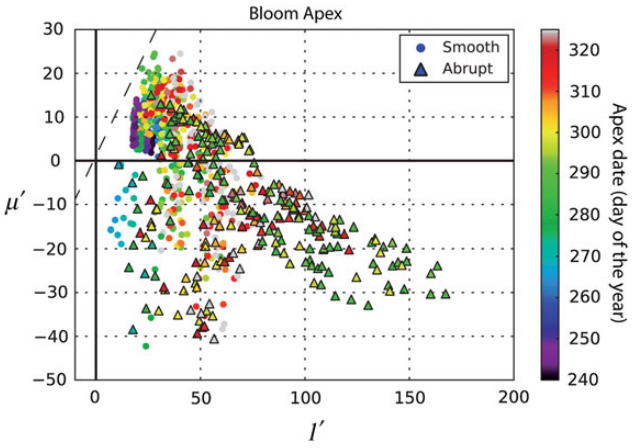

Figure 8. Growth and losses rate trends at the date of the apex for the ensemble of modelled blooms. Circles stand for smooth blooms and triangles for abrupt blooms. The absolute apex date (day of the year) is represented by coloured symbols.

The biomass-based bloom detection method (P^*-method; see Section Methods for details) detects dates that coincide, for 85% of blooms, to the onset computed from the full vertical profile (Figure 9a). This result is not surprising given the model set-up: in our model, the mixing layer is very strongly mixed, so we expect P to be relatively constant over XLD and very weak below the mixing layer (so $P^* \approx P$). The accuracy of the P^*-method is therefore strongly tied to the choice of the mixing depth over which P^* is computed: it must be a strongly mixed surface layer which is not always well described by typical mixed-layer depth criterion (e.g. Taylor and Ferrari, 2011). Arguably, P^*-method will work better during the convective phase of the surface layer, when mixed-layer actively mixes. The P^*-method detects onset dates ~2 months before the climax

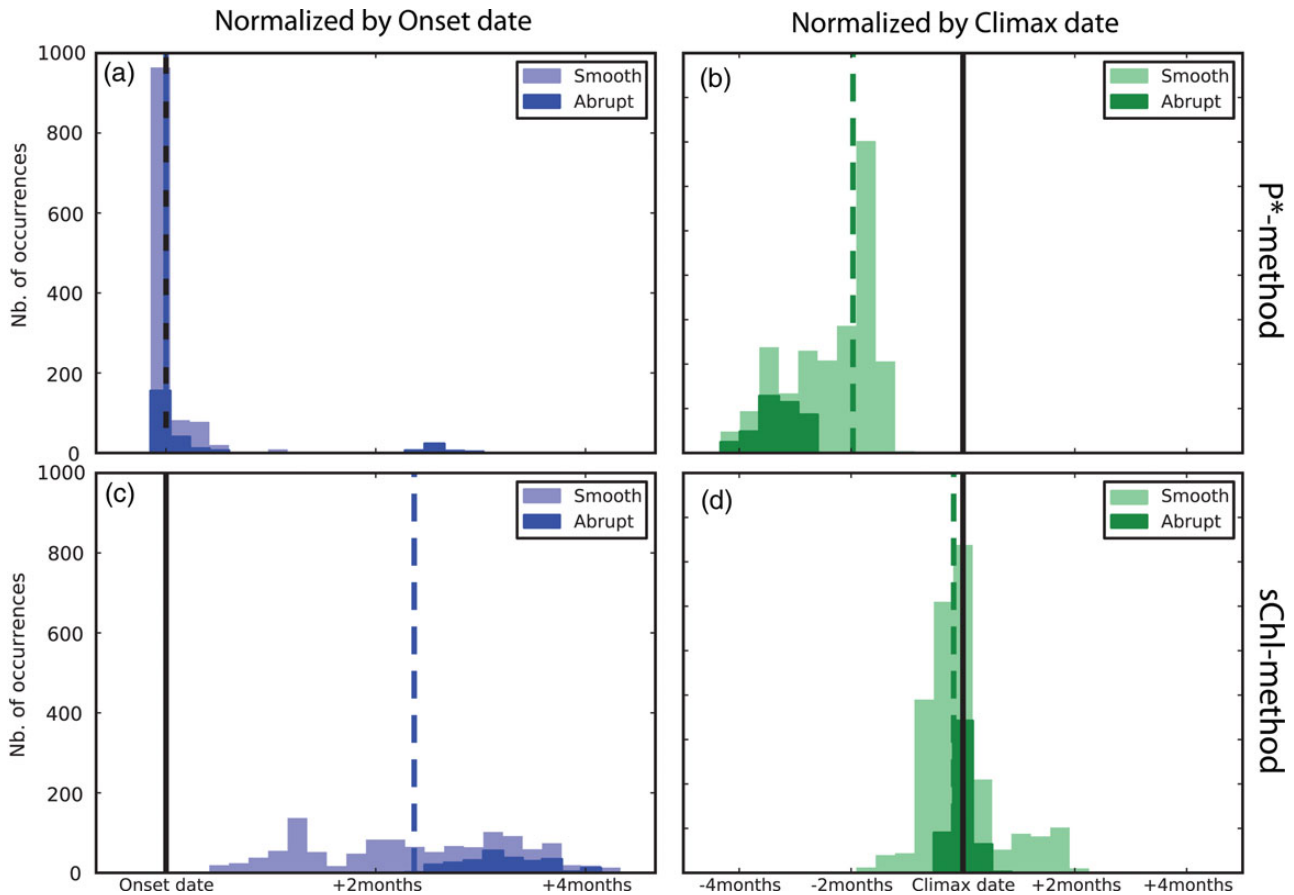

Figure 9. The histogram of the ensemble of modelled blooms representing: (a) bloom detection date using P^*-criterion normalized to the actual onset date, (b) bloom detection date using sChl-criterion normalized to the actual onset date, (c) bloom detection date using P^*-criterion normalized to the actual climax date, (d) bloom detection date using sChl-criterion normalized to the actual climax date. Median value is represented by a vertical dashed line. Abrupt blooms distribution are in dark colour and smooth blooms distribution in light colour.

(Figure 9b), in agreement with the typical time difference found between onset and climax (Figure 5a and c). On the other hand, the sChl-method detects dates that are only very weakly related to the actual onsets in our model scenarios (Figure 9c). Onset dates derived from this method are 1–4 months later than the actual onset, with a median value of ~2.5 months later. Interestingly, the dates detected by sChl-method are more closely related to the bloom climax (Figure 9d), with this bias even clearer for abrupt blooms (dark green on Figure 9d).

From these results, we conclude that, usually, the P^*-method is reliable on detecting the bloom onset while the sChl-method mainly detects the bloom climax.

Evaluating Sverdrup's bloom conditions from space

A significant part of the recent works that contributed to the bloom onset debate is based on ocean-colour data (Siegel, 2002; Behrenfeld, 2010; Chiswell, 2011). However, some authors have shown how bloom detection from ocean-colour data may be strongly influenced by the time-series data gaps (Cole *et al.*, 2012) and specially by the detection method applied (Ji *et al.*, 2010; Brody *et al.*, 2013). With the aim to evaluate at which point the choice on the detection method influence the validation or refusal of the Sverdrup (1953)'s hypothesis, here used model data to compare the dates of bloom detection with the bloom onset date predicted by the critical depth hypothesis (Figure 10). Such a comparison was done in a similar way as for bloom phases: normalizing the dates of detection by the date at which *XLD* reaches the critical depth (i.e. $XLD = Z_c$).

This comparison shown that the P^*-method detected dates 2–4.5 months before Sverdrup (1953)'s conditions were satisfied (median value ~3.6 months before; Figure 10a). Similarly, close to 95% of the dates associated with sChl-method were before *XLD* became shallower than Z_c. However, for abrupt blooms, the dates detected by the sChl-method were well distributed around the XLD $= Z_c$ date (Figure 10b, black bars).

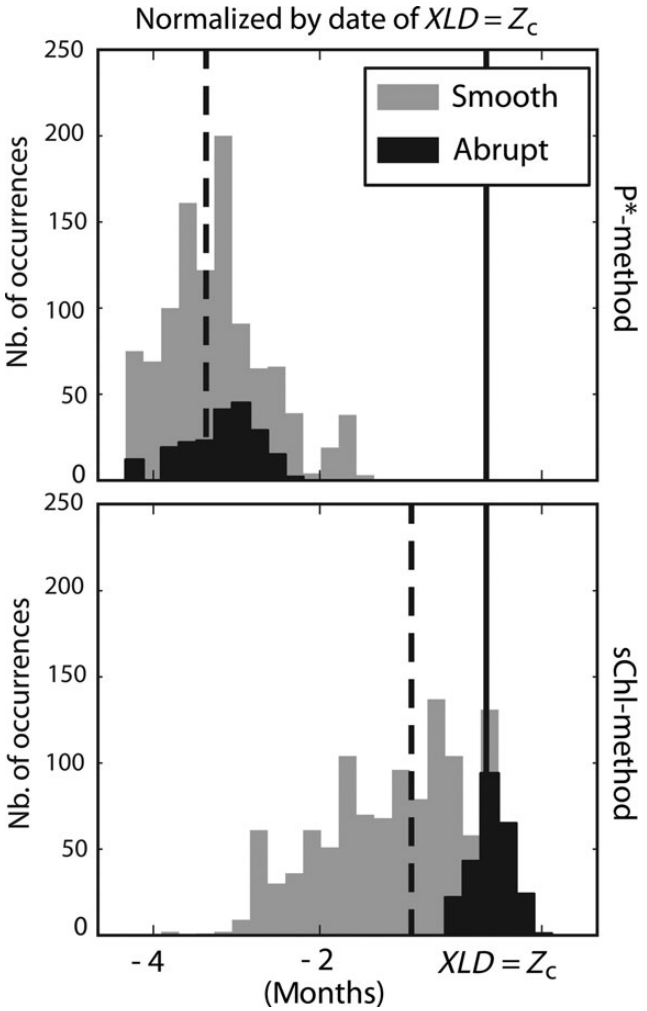

Figure 10. The histogram of the ensemble of modelled blooms representing: (a) bloom detection date using P^*-criterion normalized by the date at which Sverdrup's conditions are satisfied, (b) bloom detection date using sChl-criterion normalized by the date at which Sverdrup's conditions are satisfied. Median value is represented by a vertical dashed line. Abrupt blooms distribution are in dark colour and smooth blooms distribution in light colour.

Discussion

During the last 20 years, many studies based on SO bloom dynamics have been conducted. Most of them rely on satellite ocean-colour observations (Moore *et al.*, 1999; Venables *et al.*, 2007; Fauchereau *et al.*, 2011) except specific locations where mooring observations have been sampled (Jeandel *et al.*, 1998; Abbott *et al.*, 2000; Weeding and Trull, 2013), occasional oceanographic surveys (Boyd *et al.*, 2000; Pollard *et al.*, 2007; Blain *et al.*, 2007), and recent datasets obtained by elephant seals equipped with CTD and fluorescence sensors (Blain *et al.*, 2013). While *in situ* observations usually offer water column measurements, they are limited to specific regions and last for only a few weeks/months. In contrast, satellite-based chlorophyll data provide substantial spatial and temporal coverage. However, they are limited to interpret bloom dynamics solely based on its surface imprint.

Satellite-based analysis of high-latitude bloom onset often relate the increase of surface chlorophyll to the stratification of the mixed layer in spring. From this temporal correlation, authors conclude that alleviation of light limitation in the surface ocean layer is the main bloom trigger (Nelson and Smith, 1991; Siegel, 2002). Such results are based on the seminal concepts of Gran and Braarud (1935) and Riley (1942) and theoretically supported by Sverdrup's hypothesis (Sverdrup, 1953). More recently, combined analyses of satellite and model data identified onset based on its "strict" definition: the date at which integrated gains overcome losses (Behrenfeld, 2010). In this case, onset is systematically found in winter presumably caused by a fast decrease on grazing pressure during *MLD* deepening. This apparent inconsistency between the two results is subject to much debate (Chiswell, 2011; Behrenfeld and Boss, 2013; Ferrari *et al.*, 2014).

Our results shed light on the current debate by describing the bloom as a sequence of three distinct phases: an onset, a climax, and an apex. While a "strict" onset definition is consistent with a winter onset (in agreement with Behrenfeld, 2010; Behrenfeld *et al.*, 2013) the surface spring bloom is associated with the climax of the integrated bloom, which is the rapid accumulation occurring after the winter onset.

One advantage of using a model approach is that it allows us to investigate the mechanisms that drive each of the bloom phases. Interestingly, two possible winter bloom triggers have been identified: grazer-prey dilution and winter net growth (Figure 6). In addition, we find that dilution is only efficient when the destratification of the mixing layer is not too fast. When destratification is rapid, grazers are diluted, but the phytoplankton growth is reduced even

more strongly due to light limitation. In such cases, the winter onset is delayed to later in the season, when light conditions improve following the winter solstice. Furthermore, the climax phase is clearly bottom-up controlled and is the only phase of the bloom for which we identified a significant role of iron (enhancing the speed at which phytoplankton accumulates). Finally, the date at which net accumulation stops (i.e. the apex) is strongly top-down controlled (Figure 8). The complete recoupling and the thereafter readjustment is influenced by many complex biogeochemical processes involving remineralization, aggregation of particles or virus infection (Boyd *et al.*, 2012). We want to stress here that any given model, even if containing a significant level of complexity, would be suspect in the representation of these processes, which are still poorly understood. This is particularly true in the SO, where the complex cycle of iron is involved.

To complement the idealized study on the bloom dynamics and with the aim to evaluate our conclusions in satellite-based studies, we showed that it is possible to differentiate onset and climax phases using two different bloom detection methods (Figure 9a and b). In Sallée *et al.* (2015) (in this issue), these two detection methods have been used to estimate onset and climaxes dates from ocean-colour data in the SO. However, it must be noted here that (as discussed in Chiswell, 2013; Sallée *et al.*, 2015) the method proposed to detect the onset ($P^* = MLD \times sP$, Behrenfeld, 2010) can only be successfully applied during winter destratification if three conditions are satisfied: ocean-colour satellite data are available in winter, the timing and magnitude of *MLD* can be accurately estimated, and the *MLD* is actively mixed (i.e. $MLD \approx XLD$).

In the final part of this paper, we investigated at which point bloom detection methods agree with critical depth hypothesis. To do so, we computed the critical depth (Z_c) using model outputs and we compared the date at which *XLD* crosses Z_c to the dates of bloom detection. Our results showed that Sverdrup (1953)'s blooming conditions coincided well with the dates detected by sChl-method for the case of abrupt blooms (Figure 10b), and hence with the climax phase (which was proven to be mainly top-down driven; Figure 7). Altogether, our results suggest that the top-down mechanisms identified by Gran and Braarud (1935), Riley (1942), and Sverdrup (1953) are not indicative of the bloom onset, but they are still crucial to bloom dynamics as they presumably control the climax phase. We therefore suggest that much of the debate regarding winter vs. spring onset mostly results from confusions on the definition of the word "onset". It must be emphasized to note that what originally made blooms such an attractive phenomenon was "the sudden appearance of an enormous numbers of diatoms in early spring" (Bigelow, 1926). Therefore, in our opinion, the key phase of the bloom is arguably the climax, not the onset. Indeed, it is the bloom climax (and its associated surface signal) what actually defines the observed spatial heterogeneity of SO blooms (Thomalla *et al.*, 2011). We conclude then that the observed differences on spatial distribution of surface spring blooms between the North Atlantic and the SO regions are indicative of differences on the factors that control the climax phase; i.e. the *XLD* dynamics in spring and the nutriment limitation (iron for the SO). This conclusion is coherent with the fact that these two factors, and specially the coupling between them, present unique characteristics in the SO (Tagliabue *et al.*, 2014).

Our results and conclusions are based on an idealized model where strong assumptions were applied to minimize the degrees of freedom and ease results interpretation. These simplifications and assumptions must be taken into account when interpreting the results. First of all, the seasonal cycle is modelled in a 1D water column where lateral advection is not considered. Even if this may have important consequences on nutrients/iron transport, our approach is supported by recent works on iron supply in the SO (Tagliabue *et al.*, 2011, 2014). Second, in our model vertical mixing is assumed to be very strong and homogeneous from the surface to a depth level (*XLD*) and very low below. This highly turbulent mixing layer is a reasonable assumption for the SO where winds are generally strong and sustain efficient turbulent vertical mixing. However, we did not address the sources of vertical mixing and the possible sub-seasonal variations in mixing. We note here that in the present study we analysed bloom in relation to the mixing layer depth (*XLD*) which is not necessarily the same as the mixed-layer depth. While Sverdrup (1953) referred to the seasonal thermocline (classically associated to the mixed layer), recent studies have focused the interest on the upper-layer mixing (based on the critical turbulence hypothesis of Huisman *et al.*, 1999) and the mechanisms able to reduce it: positive heat fluxes (Taylor and Ferrari, 2011; Ferrari *et al.*, 2014), wind reduction (Chiswell, 2011), or sub-mesoscale eddies (Lévy *et al.*, 2001; Mahadevan *et al.*, 2012). In our study, we avoided such controversy by imposing a very strong mixed upper-layer with no sub-seasonal variability. In the real ocean (and especially in the SO), the phytoplankton activity (and therefore, the bloom dynamics) is highly affected by atmospheric and oceanic physical events ranging from synoptic (Waniek, 2003) to sub-mesoscale (Swart *et al.*, 2014) scales and from day to week. Such events are arguably an important source of variability when addressing the phytoplankton seasonal cycle with ocean-colour satellite data.

The idealized seasonal cycle of *XLD* used in this study is based on Argo observations and present three main phases during the seasonal cycle: a deepening phase (autumn–winter), a quicker shallowing phase (spring) and a transition phase (in summer) between the shallowing and the deepening. This transition phase present stable or slightly decreasing *MLD* (Sallée *et al.*, 2010; Figure 1c). However, the evolution of *XLD* throughout the seasonal cycle is actually more complex in the SO (e.g. Swart *et al.*, 2014), with short (i.e. sub-seasonal) and rapid (days to weeks) deepening/shallowing events. Such events are likely to influence the integrated accumulation of phytoplankton and the dates at which the onset, climax, and apex are reached. Among the three phases, the climax is by far the most sensitive to rapid changes on stratification (Figure 7). On the other hand, our results suggest that sub-seasonal *XLD* variability may weakly affect the onset and apex dates. The reason is that onset and apex controls (grazers dilution or low net growth for the former, and grazing pressure for the latter) are mainly related to the phytozooplankton coupling which is much less sensitive to rapid (∼day) changes in mixing depth.

Finally, it must be emphasized to point out that in our set of experiments the limiting nutrient was always dissolved iron while is known that in Fe-rich water of the SO, diatoms can also be limited by silicic acid (Boyd and Ellwood, 2010). We therefore note that our results should not be extrapolated to any other location or SO regions where main iron supply is not winter mixing (in the lee of Island and shallow plateaus), where silicic acid is a limiting factor, nor to higher latitudes (>70°S) where the role of light and ice seasonal cycle can be critical on the phytoplankton bloom phenology.

Conclusions

Implementing an ensemble of >1200 idealized physical scenarios for an isolated water column, a complex biogeochemical model has been forced with the aim to reproduce the plankton seasonal cycle for a collection of open waters/ice-free SO spots. Daily frequency model outputs covering a large spectra of the variables involved in the phytoplanktonic bloom allowed us to target the question of bloom formation mechanisms from different focus.

Three crucial stages of bloom seasonal evolution have been defined: onset, climax, and apex date. All onsets occurred in winter and a large majority (~80%) of the climax, in spring. For the onset, upper-layer mixing (or *XLD*) appeared as a key component on tilting the system to be bottom-up or top-down controlled. For climax, the amount of Fe (and thus the relative depth between mixing layer and ferricline) seemed to play a secondary but significant role on the intensity of accumulation. Concerning apex, permanent top-down control was identified.

Two bloom detection criteria were tested using model surface chlorophyll and mixed-layer integrated biomass estimated from surface values. The biomass-based method appeared as a good proxy for detecting bloom onset while the method based on surface chlorophyll was reliable on detecting the climax. Finally, we compared the date at which *XLD* crosses the critical depth with the dates of bloom detection by the biomass- and the sChl-based methods. Sverdrup (1953)'s blooming conditions fairly coincided with the dates of detection using the sChl-method, and therefore with the bloom climax.

Our results suggest the existence of bottom-up as well as top-down drivers of the different phases of the blooms. It also enlightens the apparent controversy between onset/surface bloom detection and it shows that how different criteria can be used to answer different questions.

Acknowledgements

The authors thank J. LeSommer and L. Bopp for their suggestions, comments, and discussions at several stages of this study. We are grateful to A. Albert, C. Ethé, S. Ayata, and O. Aumont for their invaluable help on the technical aspects and setting up of model configuration. This study was possible thanks to the research staff exchange SOCCLI program (FP7-PEOPLE-2012-IRSES). We also thank the two anonymous reviewers for their comments that improved the final manuscript.

References

Abbott, M. R., Richman, J. G., Letelier, R. M., and Bartlett, J. S. 2000. The spring bloom in the Antarctic polar frontal zone as observed from a mesoscale array of bio-optical sensors. Deep Sea Research Part II: Topical Studies in Oceanography, 47: 3285–3314.

Arrigo, K. R., van Dijken, G. L., and Bushinsky, S. 2008. Primary production in the southern ocean, 1997–2006. Journal of Geophysical Research, 113: C38004.

Aumont, O., and Bopp, L. 2006. Globalizing results from ocean in situ iron fertilization studies. Global Biogeochemical Cycles, 20: GB2017.

Banse, K. 1994. Grazing and zooplankton production as key controls of phytoplankton production in the open ocean. Oceanography, 7: 13–20.

Behrenfeld, M. J. 2010. Abandoning Sverdrup's critical depth hypothesis on phytoplankton blooms. Ecology, 91: 977–989.

Behrenfeld, M. J., and Boss, E. S. 2013. Resurrecting the ecological underpinnings of ocean plankton blooms. Annual Review of Marine Science, 6:167–194.

Behrenfeld, M. J., Doney, S. C., Lima, I., Boss, E. S., and Siegel, D. A. 2013. Annual cycles of ecological disturbance and recovery underlying the subarctic Atlantic spring plankton bloom. Global Biogeochemical Cycles, 27: 526–540.

Bigelow, H. B. 1926. Plankton of the offshore waters of the Gulf of Maine. US Government Printing Office, 40: 1–509.

Blain, S., Quéguiner, B., Armand, L., Belviso, S., Bombled, B., Bopp, L., Bowie, A., *et al.* 2007. Effect of natural iron fertilization on carbon sequestration in the southern ocean. Nature, 446: 1070–1074.

Blain, S., Sophie, R., Xiaogang, X., Hervé, C., and Christophe, G. 2013. Instrumented elephant seals reveal the seasonality in chlorophyll and light-mixing regime in the iron fertilized southern ocean. Chlorophyll and light in Southern Ocean. Geophysical Research Letters, 40: 6368–6372.

Boss, E., and Behrenfeld, M. 2010. In situ evaluation of the initiation of the North Atlantic phytoplankton bloom. Geophysical Research Letters, 37: L18603.

Boyd, P., Watson, A., Law, C., Abraham, E., Trull, T., Murdoch, R., Bakker, D., *et al.* 2000. A mesoscale phytoplankton bloom in the polar southern ocean stimulated by iron fertilization. Nature, 407: 695–702.

Boyd, P. W., and Ellwood, M. J. 2010. The biogeochemical cycle of iron in the ocean. Nature Geoscience, 3: 675–682.

Boyd, P. W., Strzepek, R., Chiswell, S., Chang, H., DeBruyn, J. M., Ellwood, M., Keenan, S., *et al.* 2012. Microbial control of diatom bloom dynamics in the open ocean. Geophysical Research Letters, 39: L18601.

Broderau, L., Treguier, A. M., Penduff, T., and Gulev, S. 2008. An ERA40-based atmospheric forcing for global ocean circulation models. Ocean Modelling, 31: 88–104.

Brody, S. R., Lozier, M. S., and Dunne, J. P. 2013. A comparison of methods to determine phytoplankton bloom initiation. Journal of Geophysical Research: Oceans, 118: 2345–2357.

Buitenhuis, E. T., and Geider, R. J. 2010. A model of phytoplankton acclimation to iron-light colimitation. Limnology and Oceanography, 55: 714–724.

Chiswell, S. 2011. Annual cycles and spring blooms in phytoplankton: don't abandon Sverdrup completely. Marine Ecology Progress Series, 443: 39–50.

Chiswell, S. M. 2013. Comment on "annual cycles of ecological disturbance and recovery underlying the subarctic atlantic spring plankton bloom". Global Biogeochemical Cycles, 27: 1291–1293.

Cole, H., Henson, S., Martin, A., and Yool, A. 2012. Mind the gap: the impact of missing data on the calculation of phytoplankton phenology metrics. American Geophysical Union, 117: C08030.

Droop, M. R. 1983. 25 years of algal growth kinetics a personal view. Botanica Marina, 26: 99–112.

Eppley, R. W. 1972. Temperature and phytoplankton growth in the sea. Fish Bulletin, 4: 1063–1085.

Evans, G. T., and Parslow, J. S. 1985. A model of annual plankton cycles. Biological Oceanography, 3: 327–347.

Fauchereau, N., Tagliabue, A., Bopp, L., and Monteiro, P. M. S. 2011. The response of phytoplankton biomass to transient mixing events in the southern ocean. Geophysical Research Letters, 38: L17601.

Ferrari, R., Merrifield, S. T., and Taylor, J. R. 2014. Shutdown of convection triggers increase of surface chlorophyll. Journal of Marine Systems, 0924-7963. http://www.sciencedirect.com/science/article/pii/S0924796314000384 (last accessed 6 April 2015).

Franks, J. S. 2014. Has Sverdrup's critical depth hypothesis been tested? Mixed layers vs. turbulent layers. ICES Journal of Marine Science, doi:10.1093/icesjms/fsu175.

Gran, H. H., and Braarud, T. 1935. A quantitative study of the phytoplankton in the Bay of Fundy and the Gulf of Maine (including observations on hydrography, chemistry and turbidity). Journal of the Biological Board of Canada, 1: 279–467.

Huisman, J., van Oostveen, P., and Weissing, F. J. 1999. Critical depth and critical turbulence: two different mechanisms for the

development of phytoplankton blooms. Limnology and Oceanography, 7: doi:10.4319/lo.1999.44.7.1781.

Jeandel, C., Ruiz-Pino, D., Gjata, E., Poisson, A., Brunet, C., Charriaud, E., Dehairs, F., *et al.* 1998. KERFIX, a time-series station in the southern ocean: a presentation. Journal of Marine Systems, 17: 555–569.

Ji, R., Edwards, M., Mackas, D. L., Runge, J. A., and Thomas, A. C. 2010. Marine plankton phenology and life history in a changing climate: current research and future directions. Journal of Plankton Research, 32: 1355–1368.

Lozier, M. S., Dave, A. C., Palter, J. B., Gerber, L. M., and Barber, R. T. 2011. On the relationship between stratification and primary productivity in the North Atlantic. Geophysical Research Letters, 38: L18609.

Lévy, M. 2015. Exploration of the critical depth hypothesis with a simple NPZ model. ICES Journal of Marine Science, doi:10.1093/icesjms/fsv016.

Lévy, M., Klein, P., and Treguier, A. M. 2001. Impact of sub-mesoscale physics on production and subduction of phytoplankton in an oligotrophic regime. Journal of Marine Research, 59: 535–565.

Lévy, M., Lehahn, Y., André, J. M., Mémery, L., Loisel, H., and Heifetz, E. 2005. Production regimes in the northeast Atlantic: a study based on sea-viewing wide field-of-view sensor (SeaWiFS) chlorophyll and ocean general circulation model mixed layer depth. Journal of Geophysical Research, 110: 1978–2012, C07S10.

Mahadevan, A., D'Asaro, E., Lee, C., and Perry, M. J. 2012. Eddy-driven stratification initiates north Atlantic spring phytoplankton blooms. Science, 337: 54–58.

Marra, J., and Barber, R. T. 2004. Phytoplankton and heterotrophic respiration in the surface layer of the ocean. Geophysical Research Letters, 31: L09314.1–L09314.4.

Martin, J. H., Fitzwater, S. E., and Gordon, R. M. 1990. Iron deficiency limits phytoplankton growth in Antarctic waters. Global Biogeochemical Cycles, 4: 5–12.

McCarthy, J. J. 1980. The kinetics of nutrient utilization. *In Physiological Bases of Phytoplankton Ecology*. Ed. by T. Piatt. Canadian Bulletin of Fisheries and Aquatic Sciences, 210: 211–233.

Moore, J. K., and Abbott, M. R. 2000. Phytoplankton chlorophyll distributions and primary production in the southern ocean. Journal of Geophysical Research, 105: 28–709.

Moore, J. K., Abbott, M. R., Richman, J. G., Smith, W. O., Cowles, T. J., Coale, K. H., Gardner, W. D., *et al.* 1999. SeaWiFS satellite ocean color data from the southern ocean. Geophysical Research Letters, 26: 1465–1468.

Nelson, D. M., and Smith, W. O. 1991. Sverdrup revisited: critical depths, maximum chlorophyl levels, and the control of southern ocean productivity by the irradiance-mixing regime. Limnology and Oceanography, 36: 1650–1661.

Pollard, R., Sanders, R., Lucas, M., and Statham, P. 2007. The Crozet natural iron bloom and export experiment (CROZEX). Deep Sea Research Part II: Topical Studies in Oceanography, 54: 1905–1914.

Riley, G. 1942. The relationship of vertical turbulence and spring diatom flowerings. Journal of Marine Research, 5.1: 67–87.

Sallée, J. B., Llort, J., Tagliabue, A., and Lévy, M. 2015. Characterisation of distinct bloom phenology regimes in the Southern Ocean. ICES Journal of Marine Science, in press.

Sallée, J. B., Speer, K., Rintoul, S., and Wijffels, S. 2010. Zonally asymmetric response of the Southern Ocean mixed-layer depth to the Southern Annular Mode. Nature Geoscience, 3: 273–279.

Siegel, D. A. 2002. The North Atlantic spring phytoplankton bloom and Sverdrup's critical depth hypothesis. Science, 296: 730–733.

Sverdrup, H. U. 1953. On conditions for the vernal blooming of phytoplankton. Journal du Conseil, 18: 287–295.

Swart, S., Thomalla, S. J., and Monteiro, P. M. S. 2014. The seasonal cycle of mixed layer dynamics and phytoplankton biomass in the sub-Antarctic zone: a high-resolution glider experiment. Journal of Marine Systems, doi:10.1016/j.jmarsys.2014.06.002.

Tagliabue, A., Mtshali, T., Aumont, O., Bowie, A. R., Klunder, M. B., Roychoudhury, A. N., and Swart, S. 2011. A global compilation of over 13 000 dissolved iron measurements: focus on distributions and processes in the southern ocean. Biogeosciences Discussions, 8: 11489–11527.

Tagliabue, A., Sallée, J. B., Bowie, A. R., Lévy, M., Swart, S., and Boyd, P. 2014. Surface-water iron supplies in the southern ocean sustained by deep winter mixing. Nature Geoscience, 7: 314–320.

Taylor, J. R., and Ferrari, R. 2011. Shutdown of turbulent convection as a new criterion for the onset of spring phytoplankton blooms. Limnology and Oceanography, 56: 2293–2307.

Thomalla, S. J., Fauchereau, N., Swart, S., and Monteiro, P. M. S. 2011. Regional scale characteristics of the seasonal cycle of chlorophyll in the southern ocean. Biogeosciences, 8: 2849–2866.

Venables, H., Pollard, R., and Popova, E. 2007. Physical conditions controlling the development of a regular phytoplankton bloom north of the crozet plateau, southern ocean. Deep Sea Research Part II: Topical Studies in Oceanography, 54: 1949–1965.

Waniek, J. J. 2003. The role of physical forcing in initiation of spring blooms in the northeast Atlantic. Journal of Marine Systems, doi:10.1016/S0924-7963(02)00248-8.

Weeding, B., and Trull, T. W. 2013. Hourly oxygen and total gas tension measurements at the southern ocean time series site reveal winter ventilation and spring net community production. Journal of Geophysical Research: Oceans, 119: 348–358.

White, M. A., de Beurs, K. M., Didan, K., Inouye, D. W., Richardson, A., Jensen, O. P., O'Keefe, J., *et al.* 2009. Intercomparison, interpretation, and assessment of spring phenology in North America estimated from remote sensing for 1982–2006. Global Change Biology, 15.10: 2335–2359.

Yoshie, N., Yamanaka, Y., Kishi, M. J., and Saito, H. 2003. One dimensional ecosystem model simulation of the effects of vertical dilution by the winter mixing on the spring diatom bloom. Journal of Oceanography, 59.5: 563–571.

Handling editor: Rubao Ji